INCREASED HYDRIDE TRANSFER RATES WITHIN T09A MUTANT OF F_{420}:H_2 $NADP^+$ OXIDOREDUCTASE

By

MD HASMAT ULLAH

THESIS

Presented to the Faculty of the Graduate School of

The University of Texas at Arlington in Partial Fulfillment

of the Requirements for the Degree of

MASTER OF SCIENCE IN CHEMISTRY

THE UNIVERSITY OF TEXAS AT ARLINGTON

May 2016

Acknowledgements

I would like to especially thank my honorable supervisor, Dr. Kayunta Johnson-Winters. Her care and guidance was really special for me. I was blessed with her continuous support, even on my toughest times. I would also like to thank my other committee members, Dr. Subhrangsu Mandal and Dr. Jongyun Heo for their valuable guidance and suggestions on my way.

I want to thank National Science Foundation (NSF) grant numbers 1120837 (to K.J.-W.) and University of Texas at Arlington for the funding support in this research.

I am really grateful to my former and current lab mates for their support. Especially, Dr. Ebenzer Joseph, Dr. Cuong Le and Mercy Oyugy for teaching me techniques from scratch. I would like to thank my friends, Siqi Du, Toan Nguyen, and all of the undergraduate researchers who worked with me- Joseph Tran, Joshua Aubert, Thien Phan, Thanh, Halie and new graduate members of our lab Lindsay Davis and Danzel Washington.

I would like to acknowledge the cordial support of all my Biochemistry friends- Monira, Paromita, Hope, Alice, Karan, Farinaz, my batch mates- Fakrul, Dananjay, Pawan and other friends- Jayanta, Shahin, Shaker, Kabir, Mohammad Hossain and many others.

Finally, I want to thank my parents, Enayet Ullah and Khaleda Parveen as well as other family members for their unconditional support on my way.

April 18, 2016

Abstract

INCREASED HYDRIDE TRANSFER RATES WITHIN T09A MUTANT OF F_{420}:H_2 $NADP^+$ OXIDOREDUCTASE

Md Hasmat Ullah, MS

The University of Texas at Arlington, 2016

Supervising Professor: Kayunta Johnson-Winters

F_{420}:H_2 $NADP^+$ oxidoreductase (Fno) is an F_{420} dependent enzyme found in methanogens and sulfate reducing archaea. Fno catalyzes the reversible reduction of $NADP^+$ to NADPH through the transfer of a hydride involving F_{420} cofactor. The focus of our work is to study the hydride transfer mechanism of Fno from *Archaeoglobus fulgidus* using site directed mutagenesis, steady-state and pre steady-state kinetic methods. Threonine 09 (T09) is a conserved residue within Fno. The hydroxyl (–OH) group of T09 interacts with the phosphate and ribose of neighboring NADPH. Therefore, T09 was converted into an alanine (T09A) to study its functionality within Fno and its affects on the donor acceptor distances between FO and NADPH. Binding studies of T09A mutant revealed that T09 does not affect the binding of FO. However, this study revealed an increased dissociation constant for NADPH, which represents decreased affinity of Fno for NADPH. Like wildtype Fno (*wt*Fno), the steady-state kinetic studies of T09A Fno with varying concentrations of the deazaflavin chromophore of the F_{420} cofactor (FO) showed typical Michaelis-Menten hyperbolic plots. However, the steady-state kinetic studies varying NADPH concentrations displayed the biphasic non-hyperbolic properties. The kinetic parameter, k_{cat} for FO is comparable with *wt*Fno , however the Michaelis-Menten constant (K_m) value was almost double than the *wt*Fno . The K_m for NADPH of the first

phase was similar to *wt*Fno. However, the data revealed a three fold increase in the K_m for the second phase. According to the steady-state data, the presence of NADPH is required prior to FO for optimal activity for the T09A variant. The pre steady-state kinetic data revealed a 36-fold increased rate of hydride transfer for the T09A variant compared to *wt*Fno. In contrast to *wt*Fno pre steady-state kinetic data, T09A displayed a single-phase exponential decay, rather than biphasic burst kinetics. These data suggest that Threonine 09 plays a role in NADPH binding, the rate at which the hydride is transferred to the FO cofactor and subunit communication within the Fno dimer.

Table of Contents

List of schemes

List of figures

List of tables

List of abbreviations

Fno	$F_{420}H_2$: $NADP^+$ oxidoreductase
NADPH	Nicotinamide adenine dinucleotide phosphate (reduced form)
*wt*Fno	Wild-type Fno
$NADP^+$	Nicotinamide adenine dinucleotide phosphate (oxidized form)
E. coli	*Escherichia coli*
FO	F_{420} cofactor precursor
LB	Luria bertani broth
K_d	Dissociation constant
k_{cat}	Michaelis-Menten catalytic rate constant (turnover number)
SDS-PAGE	Sodium dodecyl sulfate polyacrylamide gel electrophoresis
F_{420}	F_{420} cofactor
T09	Threonine 09
SAM	S- Adenosyl Methionine

Chapter 1

F_{420} Cofactor

1.1 Introduction

F_{420} cofactor is found in many different organisms such as methanogenic archaea, sulfate reducing archaea, halobacteria, *Streptomyces*, *Mycobacteria*, cyanobacteria and some eukaryotes (1–11). It acts as a two-electron acceptor in these organisms. In *Streptomyces*, F_{420} dependent enzymes are involved in carbon fixation and antibiotic biosynthesis, such as tetracyclins (12, 13) . In *Mycobacteria*, it is involved in the degradation of mycotoxins.

The first F_{420} cofactor purification was reported by Cheesemen *et al.* from *Methanobacterium* Strain M.o.H(14). After spectral analysis, it was found that, the oxidized F_{420} cofactor gives rise to a peak at 420 nm. However, upon reduction, the peak was disappeared from 420 nm and generated a new shoulder at 320 nm. Over 90% of the environmental methane has been produced by methanogenic bacteria. Methane is a very important energy source which can act also as a greenhouse gas. So understanding the mechanisms of F_{420} dependent enzymes will lead to enhance our knowledge to learn the mechanisms involved in biological methane production.

1.2 Structure of F_{420} Cofactor.

The structure of F_{420} cofactor was first solved by Eirich *et al* (15). They used IR spectroscopy, UV-Vis, ^{1}H and ^{13}C NMR and quantitative elemental analysis.

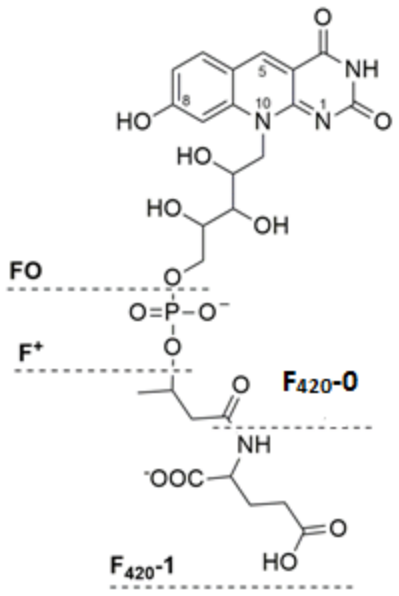

Scheme 1.1 : F_{420} cofactor with its precursors (14). The deazaflavin ring with ribitol moiety is called FO, in addition of a phosphate group it becomes F^+. Addition of lactate group makes it F_{420}-0, upon addition of each of the gamma glutamic acid it turns into F_{420}-1, F_{420}-2 and so on. The number of glutamate can be 2-9 depending on organism.

F_{420} cofactor contains a deazaisoalloxazine structure and a long chain linked to N-10, which consists of a ribitol moiety, a phosphate and lactyl group (Scheme 1.1). F_{420} cofactor also contains a chain of gamma-glutamic acid. The number of glutamic acids varies depending upon the source organism. However, it is limited within 2-9. The deazaisoaloxazine chromophore attached with ribitol moiety is known as FO. Upon phosphorylation of FO, the structure is known as F^+. Once the lactyl group is added to the F^+, it becomes F_{420}-0 and with one glutamic acid it's F_{420}-1 and so forth. The cofactor isolated from *Methanobacterium thermoautotropicum* shows F_{420}-2 structure. However, the work of Bair *et al*. (16) showed that *Mycobacteria* species contains 5-7 glutamate residues connected to lactate group of F_{420} through γ-glutamyl linkage.

1.3 Spectral properties of F_{420} cofactor.

F_{420} cofactor has oxidized and reduced forms that give rise to distinct absorbance features (Figure 1.1). The oxidized cofactor displays absorbance at 420 nm. After reduction, the absorbance at 420 nm is depleted and a generates absorbance at 320 nm. The ionization of hydroxyl group at C10 (pKa 6.3) converts the cofactor into an anionic form, which shows two resonating forms (Scheme 1.2).

The absorbance of F_{420} cofactor is pH dependent. The 420 nm absorbance is lost at lower pH levels. The hydroxyl (–OH) group (pKa 6.3), deprotonates at lower pH and forms its anionic structure (Scheme 1.2). This anionic form has two resonating structure (B and C). The combination of these two resonance forms is responsible for the shift of the absorbance wavelength. The –NH group at 3 position (pKa 12.3) deprotonates at basic pH (structure D) and shift the absorbance wavelength as well.

The fluorescence characteristics of the F_{420} cofactor is also pH dependent. The oxidized cofactor has a strong fluorescence intensity at 425 nm. However, the reduced cofactor does not display any fluorescence. The F_{420} cofactor is also photosensitive. It decomposes rapidly upon exposure to strong white light.

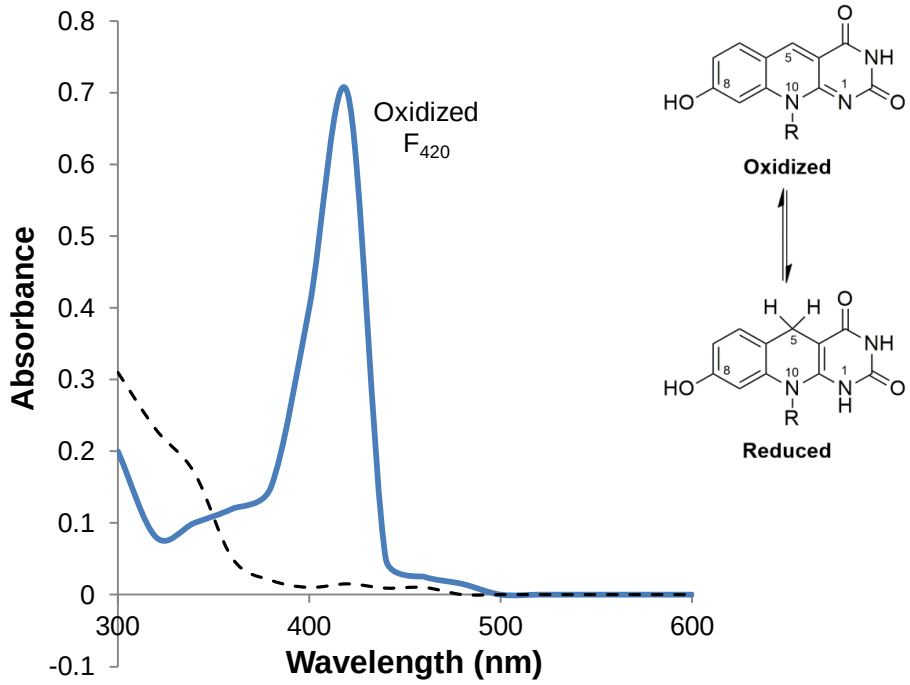

Figure 1.1: Visible spectra of oxidized and reduced F_{420} cofactor along with their corresponding structures (17).

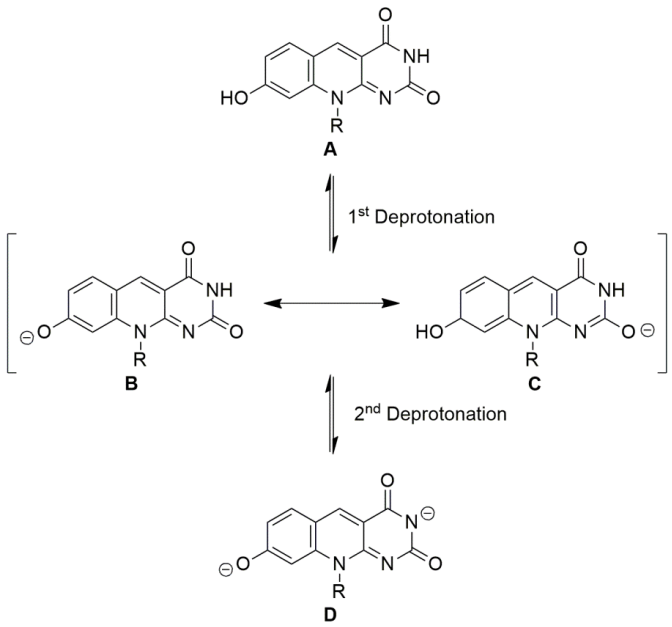

Scheme 1.2: Ionization and resonance structure of F_{420} cofactor.

1.4 F_{420} dependent enzymes.

Isolation of the F_{420} cofactor was first reported at 1972 from a methanogenic archaea (14). It was initially thought to be a unique feature of this organism. However, it was later determined to be present in other organisms such as *Streptomyces*, *Mycobacteria*, green algae and cyanobacteria. A list of the F_{420} cofactor dependent enzymes is given below. Factor F_{390} dependent enzymes are also included in this list because this cofactor converts into F_{420} under anaerobic conditions.

i. F_{420}-reducing hydrogenase (3, 18–20).
ii. F_{420}-dependent formate dehydrogenase (21).
iii. F_{420}-dependent methylenetetrahydromethanopterin dehydrogenase (9, 22, 23).
iv. F_{420}-dependent methylenetetrahydromethanopterin reductase (9, 24).
v. $F_{420}H_2$ dehydrogenase complex (9, 25).

vi. $F_{420}H_2$: $NADP^+$ oxidoreductase (3, 9, 26).

vii. F_{420}-dependent secondary alcohol dehydrogenase (22, 27).

viii. Glucose-6-phosphate dehydrogenase (28).

ix. F_{420}-dependent DNA photolyase (29–33).

x. Coenzyme F_{390} synthetase (34, 35).

xi. Coenzyme F_{390} hydrolase (36, 37).

xii. $F_{420}H_2$ oxidase (38).

1.5 Reduction potential.

F_{420} cofactor has a reduction potential of -350 mV, which is more negative than $NADP^+$ (-320 mV) or FAD (-220 mV) (Figure 1.2). Therefore, F_{420} cofactor can be used as a more powerful reducing agent within the cells than any other cofactors (39).

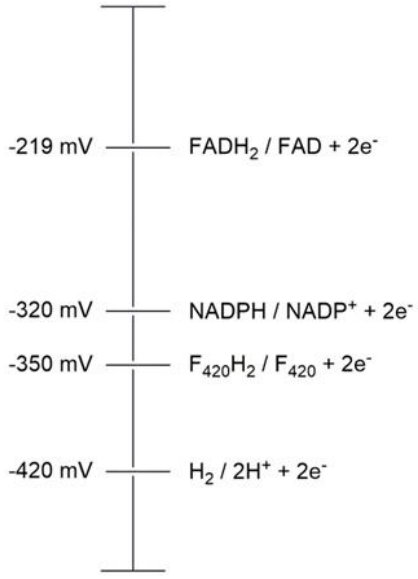

Figure 1.2: Reduction potential ladder showing the position of $F_{420}H_2$ /F_{420} redox couple (-350 mV) in comparison with other physiological electron donors (H_2) and other electron mediating entities (NADP, FAD) (8).

1.6 Biosynthesis of F_{420} cofactor.

F_{420} cofactor is biosynthesized in methanogenic archaea, as well as the bacterial sources that utilizes this cofactor. The biosynthesis of this cofactor was reported from *Methanocaldococcus jannaschii* (40). It occurs through several enzymatic reactions (40), where FO synthase plays a key role. It consists of two subunits encoded by CofG and CofH gene. Decamps. *et al*. (41) revealed that FO synthase utilizes tyrosine and 5-amino-6-ribitylamino-2,4(1H,3H)-pyrimidinedione as substrates (Scheme 1.3). There is no involvement of 4-hydroxyphenylpyruvate, which was previously suggested as one of the substrates. They found that FO synthase generates two 5'-deoxyadenosyl radical for catalysis. This has never been observed within any reactions catalyzed by SAM (S-Adenosyl methionine) enzymes.

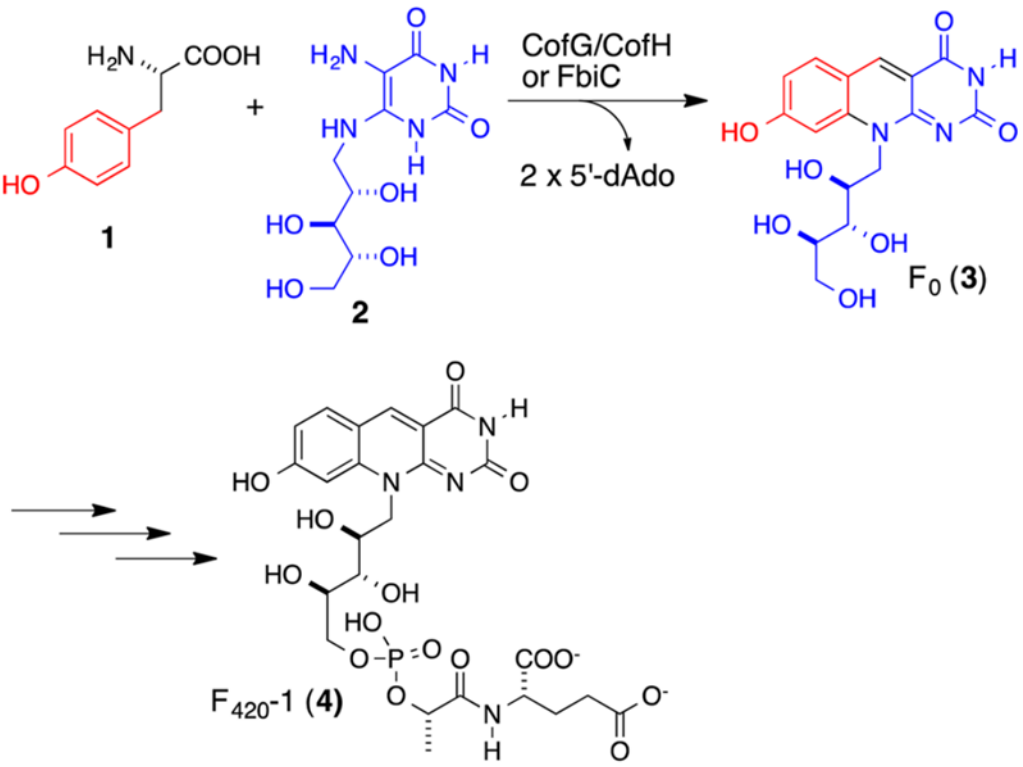

Scheme 1.3: Biosynthesis of FO (no. 3), the deazaflavin chromophore of F_{420} cofactor, (41). Here, F_{420} cofactor showed as with single glutamate (no. 4) which may be varied in different organisms. CofG and CofH are the genes code for two subunits of FO synthase enzyme, FbiC gene also involved in FO synthase enzyme, dAdo stands for deoxyadenosyl radical.

Philmus *et al*. (42) investigated the mechanism of FO synthase in F_{420} cofactor biosynthesis. FO synthase is an unusual multi-domain SAM enzyme, which uses radicals CofG and CofH for the reductive condensation of tyrosine and ribityl-diamino-uracil (Scheme 1.4). The mechanism behind the incorporation of two highly reactive SAM radical to form the deazaflavin chromophore is not well understood.

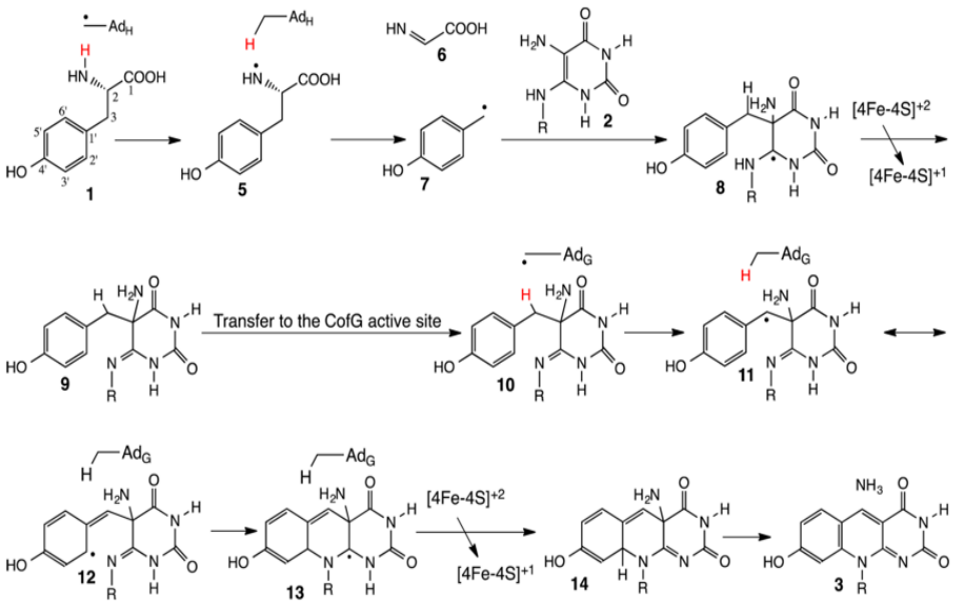

Scheme 1.4: Proposed mechanism of the FO synthase enzyme in FO biosynthesis (42). AdG and AdH represent to 5'- deoxyadenosyl radicals generated at the active sites of CofG and CofH by reduction of SAM with the help of $[4Fe\text{-}4S]^{+1}$ cluster. Abstraction of hydrogen from the amine group of tyrosine yields 5, which then forms radical 7 via fragmentation. Addition of diamino uracil to the radical gives 8, followed by oxidation to give 9. Transfer of 9 to the active site of CofG gives 10, abstraction of hydrogen by AdG gives radical 11, which cyclizes into 13, then oxidized into 14 via $[4Fe\text{-}4S]^{+2}$. Elimination of ammonia from 14 completes the synthesis of deazaflavin 3.

1.7 Organic synthesis of FO.

Organic synthesis of the F_{420} precursor, FO was reported by Yoneda *et al* (Scheme 1.5). Then, in 1976 Ashton *et al*. reported F_{420} cofactor synthesis (43, 44). However, the intermediates of their proposed synthesis were extremely unstable. In 2015, Hossain *et al*. developed a method for convenient synthesis of FO by improving the redox stability of the unstable intermediates. They used a protection strategy for 3-aminophenol to improve stability of the intermediate. This step allowed the use of normal phase chromatography instead of anaerobic ion exchange chromatography of the previous method. Flash chromatography was utilized to simplify the purification process (Scheme 1.6).

The synthesized FO was tested with *wt*Fno. The activity of FO was tested by aerobic steady-state kinetic with a saturating concentration of NADPH.

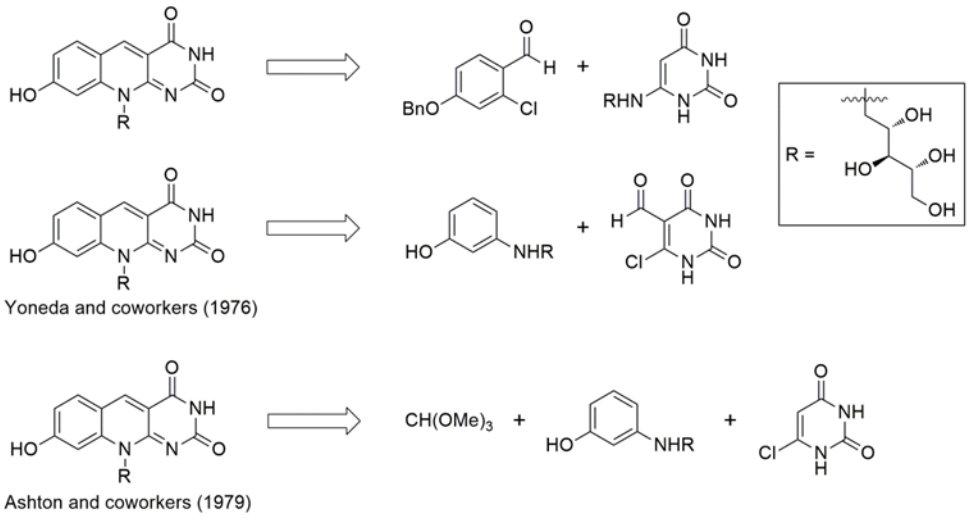

Scheme 1.5: Synthesis of FO and F_{420}, developed by Yoneda *et al*. (1976) and Ashton *et al* (1979) (43, 44).

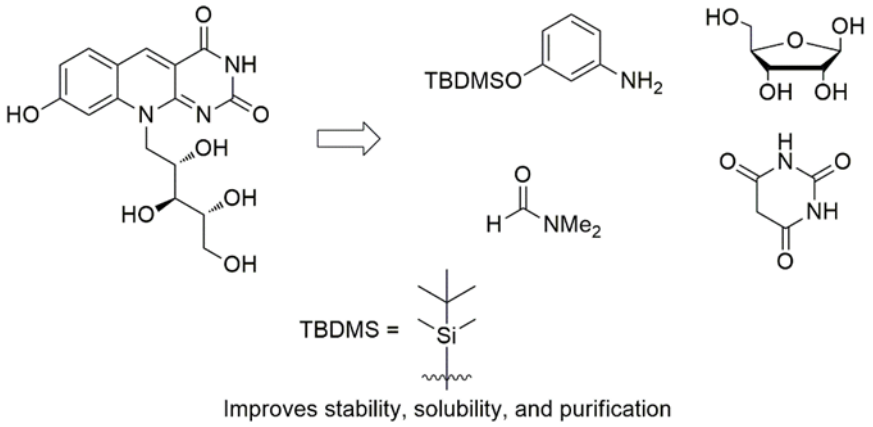

Scheme 1.6: Retrosynthesis of deazaflavin chromophore (FO) with 3-aminophenol group protection (45). TBDMS stands for the tertiary butyl dimethyl sillyl- group.

FO concentration was varied from 2 µM to 30 µM for this steady-state kinetic study. The Fno concentration was fixed (200 nM) and 50 mM MES/NaOH pH 6.5 was used as a reaction buffer. At room temperature the determined K_m for FO 4.00 ± 0.39 µM and k_{cat} was 5.27 ± 0.14 s^{-1} (Figure 1.3). The previously reported K_m for natural and oxidized F_{420} were 20 µM and 10 µM, respectively at 65 °C (9, 46). FO lacks charged polyglutamate tail of F_{420}, which would interact with the binding site of Fno. However, oxidized FO still binds tightly to the Fno in comparison to the F_{420} cofactor.

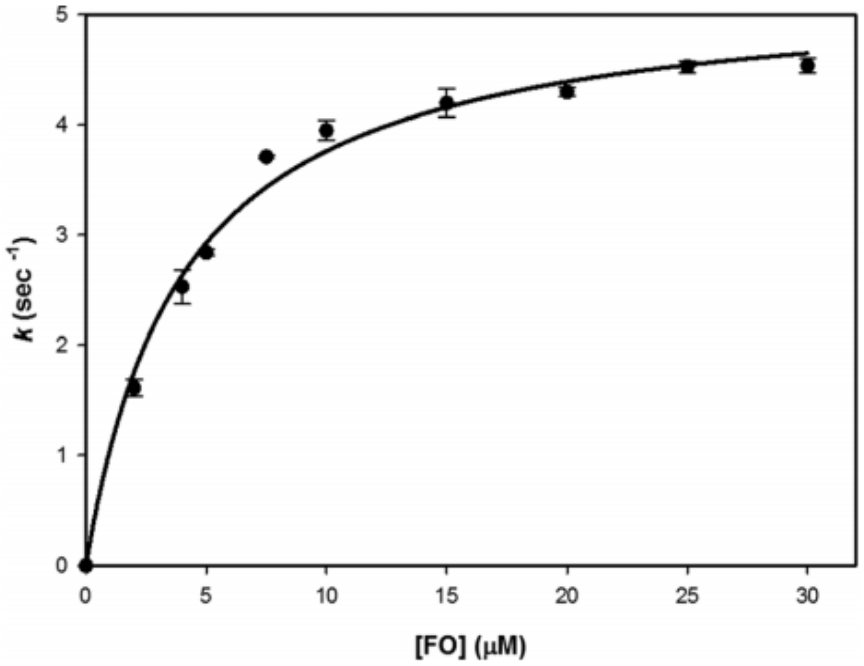

Figure 1.3: The steady-state kinetic data for Fno varying FO concentrations. The Fno and NADPH concentrations were fixed at 200 nM and 600 μM respectively. 50 mM MES/NaOH buffer pH 6.5 was used as the reaction buffer. The data is fitted into Michaelis-Menten equation ($k = k_{cat}$ [S]/(K_m+[S])).

Chapter 2

F_{420}:H_2 $NADP^+$ oxidoreductase (Fno)

2.1 Introduction.

F_{420}:H_2 $NADP^+$ oxidoreductase (Fno) is an F_{420} cofactor dependent enzyme found in methanogenic archaea and sulfate reducing archaea. Fno is responsible for the production of NADP through a reversible hydride transfer process (Scheme 2.1). Reduced F_{420} cofactor transfers a hydride from *Si*-face of F_{420} to *Si*-face of $NADP^+$, resulted the production of NADPH (3).

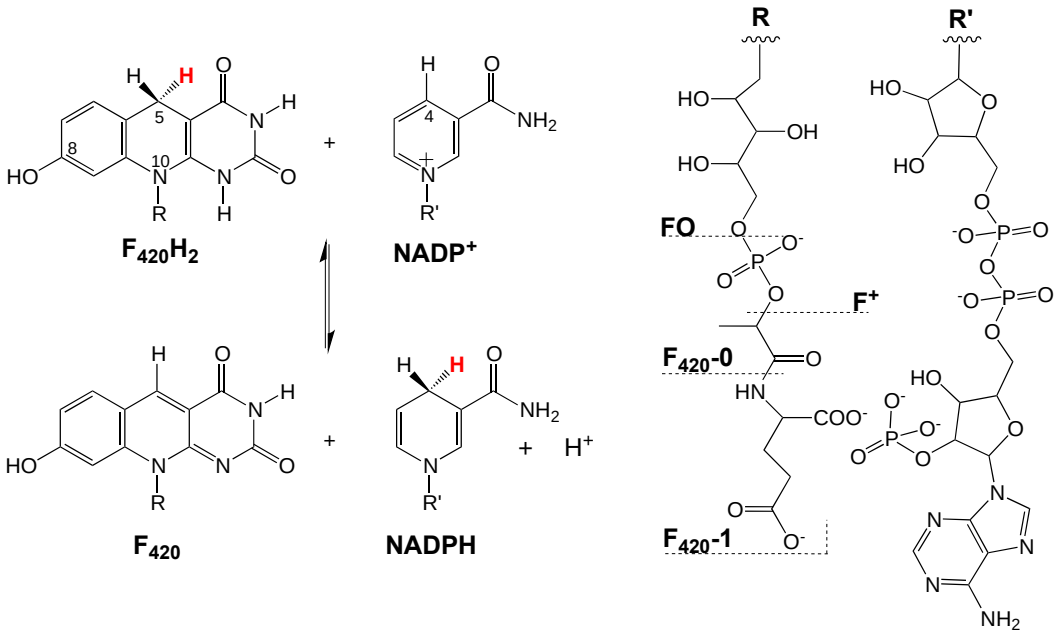

Scheme 2.1: Hydride transfer reaction catalyzed by F_{420}:H_2 $NADP^+$ oxidoreductase (Fno) (46).

2.2 Fno crystal structure

The crystal structure of Fno has been solved by Warkentin et. al.(46) from *Archaeoglobus fulgidis* at a resolution of 1.65 Å (Figure 2.1). Fno is a homodimer with an N terminal dinucleotide binding Rossman fold and a small C terminal domain. The two cofactors of Fno are are bound within the two subunits, with one NADP and one F_{420} per monomer. They are 3.1 Å apart in distance.

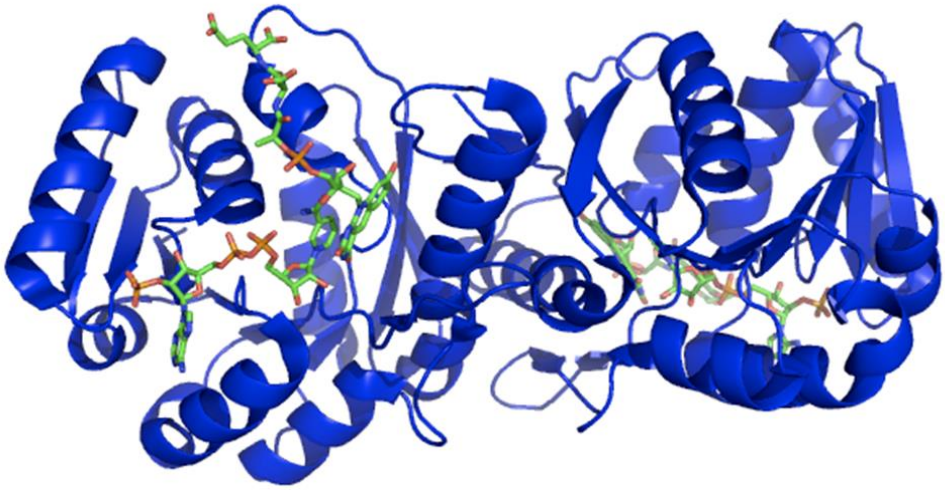

Figure 2.1: Crystal structure of F_{420}:H_2 $NADP^+$ oxidoreductase (46).

F_{420} cofactor is associated with the C terminal domain of Fno. However, the *Si*-face of deazaflavin moiety faces to the $NADP^+$.

The other coenzyme, $NADP^+$ binds to the N- terminal domain. The *Si*-face of nicotinamide ring is flanked into the *Si*-face of deazaflavin of F_{420} coenzyme (Figure 2.2). The *re*-face of the cofactor is adjacent to several hydrophobic side chains. The negatively charged phosphate group of the ribose is linked to Threonine 09 (T09), Serine 31, Arginine 32 and Lysine 36 side chains. These huge interactions between phosphate

group and side chains reflect physiological significance, which distinguishes the role of NADP and NAD in physiological system.

From the previous steady-state kinetic studies, carried out at 65 °C, a ternary complex catalytic mechanism was suggested (26). It was not possible to figure out whether the binding of two substrates are random or sequential. Warkentin *et al*. solved the crystal structure of Fno bound to the both $NADP^+$ and oxidized F_{420} cofactor (46). From the crystal structure, it is determined that the interaction of $NADP^+$ to Fno is much more extensive than the F_{420} cofactor. The distance between C4 of the deazaflavin ring and C5 of $NADP^+$ is the shortest, 3.1 Å. The distance might be reduced by bending of the substrate deazaflavin. A recent paper (51) suggested a transitional boat conformation of the pyridine part, which also could make the distance shorter (Figure 2.2).

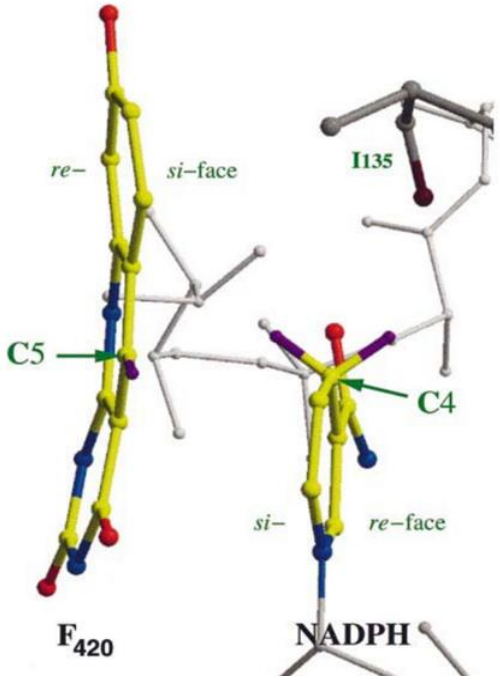

Figure 2.2: Hydride transfer from the *Si*-face of F_{420} cofactor to *Si*-face of NADPH (46).

2.3 Purification of Fno

The Fno purification was reported from several microorganisms such as *Archaeoglobus fulgidus* (46), *Methanobaterium thermoautotrophicum* (26), *Methanococcus vannielii* (3), *Methanogenium organophilum* (47), *Halobacterium cutirubrum* (48*), Methanosphaera stadtmanae* (49) and *Streptomyces griseus* (50). According to the method reported by Warkentin *et. al.,* the Fno gene was amplified by PCR, cloned into pET24b plasmid and expressed into BL21DE3 *E. coli* in control of T*lac* promoter. The recombinant bacteria were grown into a mineral salt medium at 37° C, followed by sonication to break the cells open. The sample was then heated to 90 °C for 30 minutes and passed through a 15 Phenyl column and finally a hydroxy-apatite column. Unfortunately, the purified enzyme using this protocol in our hands, displays an absorbance peak at 260 nm, which is more dominant than the protein's peak at 280 nm (Figure 2.3) (52). The peak at 260 nm suggests significant nucleic acid contamination within the enzyme. Nucleic acid contamination causes the interference with enzyme concentration determination. This contamination can lead to incorrect quantitative data and kinetic analysis. To overcome such issues, the purification protocol was optimized for Fno (52).

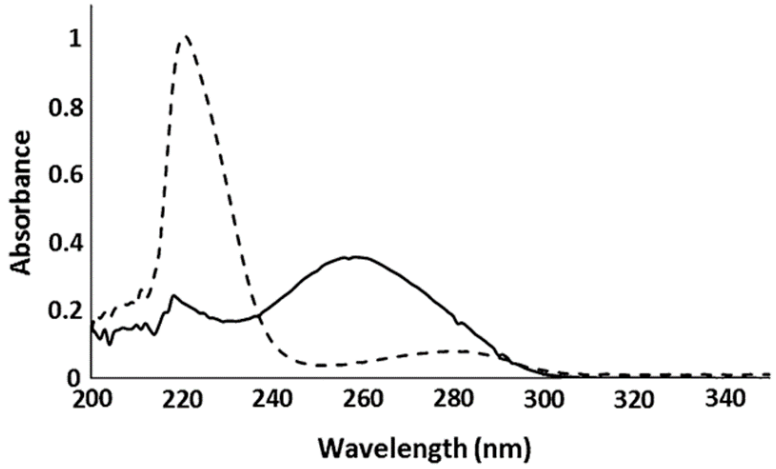

Figure 2.3: The absorbance spectra of purified Fno using previous method (Solid line) and newly developed method (dotted line) (46, 52). A dominant peak is seen at 260 nm, which interprets the presence of nucleic acid contamination.

Le *et al.* introduced a polyethyleneimine (PEI) precipitation step after ammonium sulfate precipitation, followed by anion-exchange and size exclusion chromatography to neutralize negatively charged nucleic acid through polymeric cations. The purified Fno, using this protocol was highly pure, catalytically active and free of nucleic acid contamination (Figure 2.4).

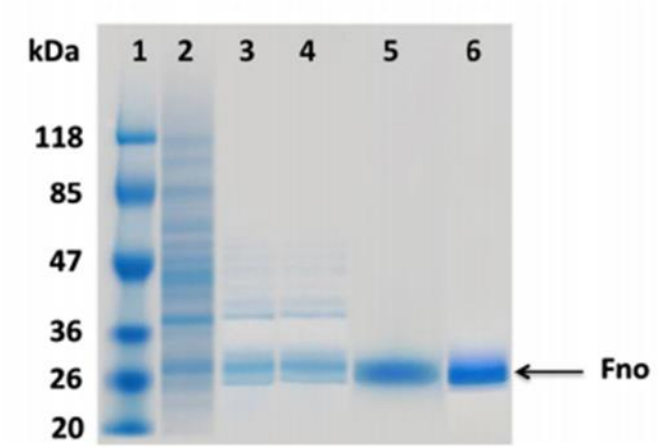

Figure 2.4: SDS gel picture of the Fno on various purification steps of improved optimized protocol (52). Lane 1 corresponds to the molecular weight marker, lane 2 for supernatant after sonication, lane 3 supernatant after heat precipitation, lane 4 re-suspended salt precipitate, lane 5 concentrated fractions after anion exchange chromatography, lane 6 is concentrated fractions after size exclusion chromatography.

2.4: Negative cooperativity within Fno

Pre steady-state spectrophotometric analysis was employed extensively to investigate kinetics of enzyme systems with highly colored cofactors, such as flavins and hemes. Fortunately, the two cofactor forms of F_{420} (oxidized and reduced) involved in the proposed work are spectrophotometrically distinct (Figure 1.1). F_{420} cofactor loses its 420-nm absorbency upon reduction and acquires a new shoulder at 320 nm. Figure 2.5 is a time trace of FO reduction within Fno at 420 nm. The reduced form of the cofactor exhibits no fluorescence, while the oxidized form does exhibit fluorescence.

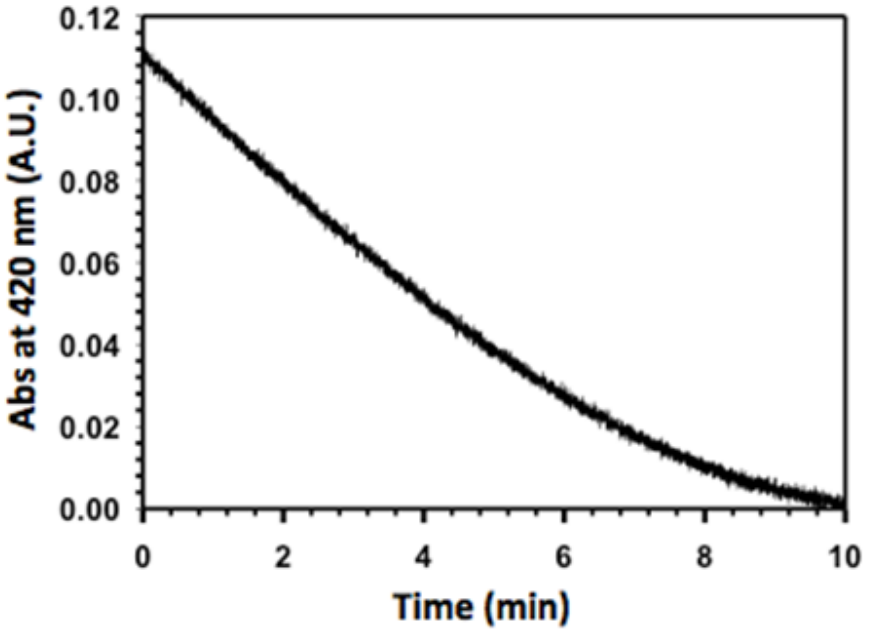

Figure 2.5: Time trace of Fno catalyzed reaction.

This serendipity permits quantitative measurement of reaction rates of Fno using standard rapid flow mixing techniques, coupled with UV-Vis detection. In this way, individual rate constants are determined. We have successfully employed this route to obtain important data on the kinetics and mechanism of the key reaction (Figures 2.5 & 2.6) of the time dependence of the absorbance changes observed with variations in enzyme concentrations. Furthermore, analysis of the pre steady-state kinetics data in terms of the initial rate FO reduction clearly reveals biphasic kinetics (Figure 2.6). At varying Fno concentrations, the fast phase, corresponds to a rate constant of 48 s^{-1}, while the slow phase was 3.4 s^{-1}. The amplitude of the initial burst phase (~50% of FO reduction) corresponding to release of product from only one of the active sites in a functional dimer (half site reactivity). Negative cooperativity is a phenomenon that is seen in different multi-subunit protein systems. It can be defined as the decreased ligand

affinity in higher ligand concentration. For the dimeric proteins (such as Fno) the affinity is higher for the first ligand, than the second ligand.

Steady-state kinetic plot of *wt*Fno varying NADPH concentration shows a non-hyperbolic character at higher concentration (Figure 2.7). The first phase (NADPH concentrations between 0-100 μM) has a lower K_m compared to the second phase and shows a steeper curve. Both phases reveal saturation kinetics, when plotted individually, which corresponds to enzyme chemistry for both phases.

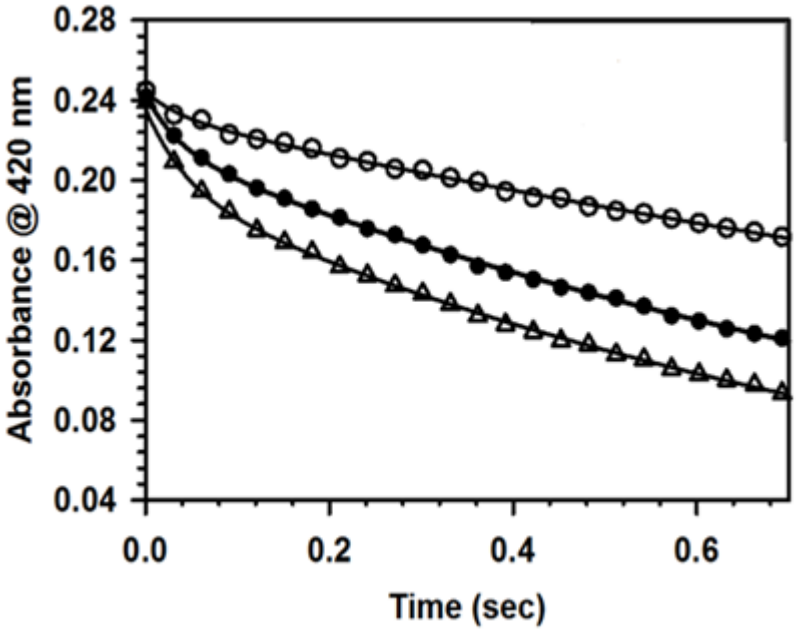

Figure 2.6: The pre steady-state kinetics of hydride transfer to FO from NADPH by Fno is shown for varying Fno concentrations – 1.5 μM (open circle), solid circle (3.0μM) and open triangle (4.0 μM).

The double reciprocal plot of NADPH steady-state data exhibits a downward concave curvature (Figure 2.8), which is indicative of negative cooperativity kinetics. The

Koshland-Nemethy-Filmer (KNF) model explained details about this characteristics of negative cooperativity. According to this model, the enzyme exists in a resting conformational in the absence of the ligand. Once a ligand binds to the first subunit of the enzyme, it results a conformational change within the unoccupied subunit (Figure 2.10). There are several examples in the literature that display either negative cooperativity or half site reactivity. **However, this has not been seen previously with Fno or other F_{420} cofactor dependent enzymes**.

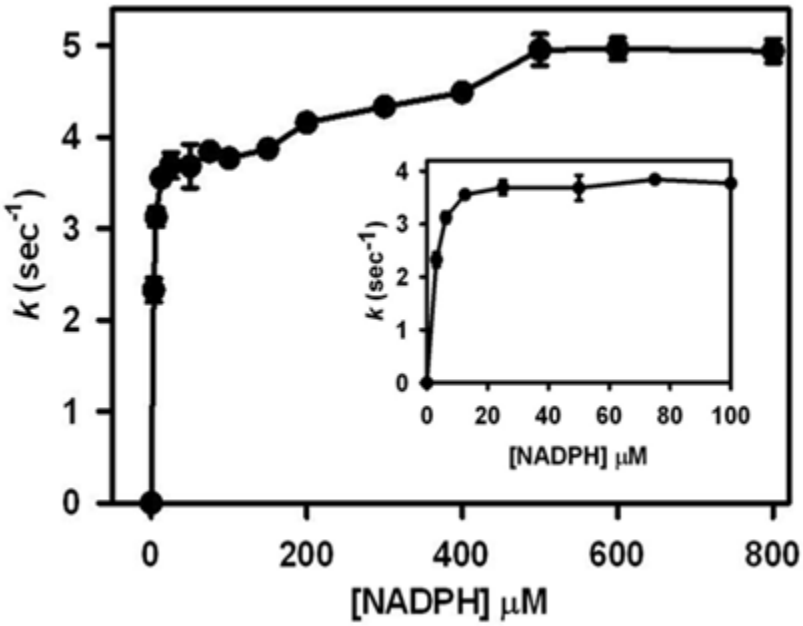

Figure 2.7: Steady-state kinetic data for *wt*Fno by varying NADPH concentrations.

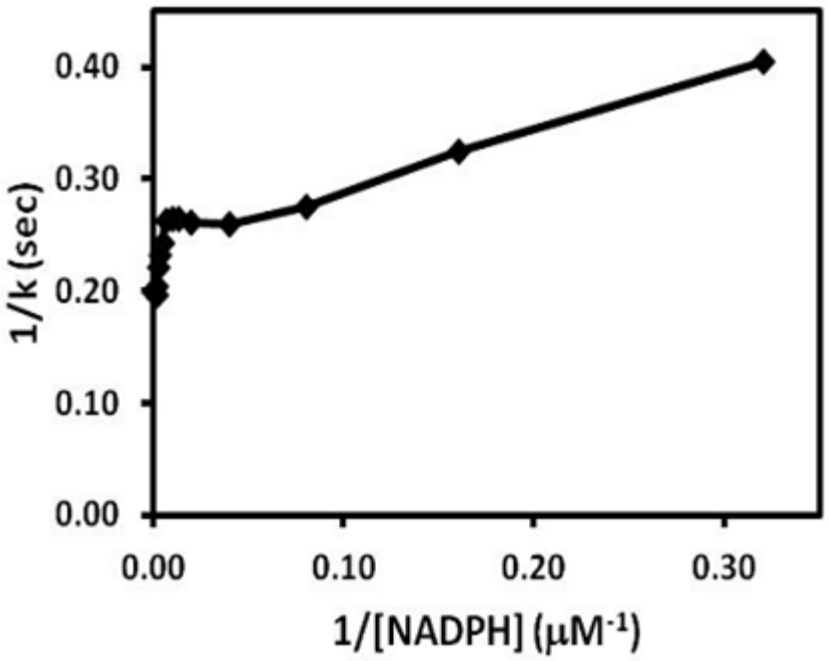

Figure 2.8: The double reciprocal plot of steady-state kinetics of *wt*Fno by varying NADPH concentrations (53).

According to the steady-state and pre steady-state kinetics described above (half-site reactivity), we proposed a mechanism of *wt*Fno enzyme (Scheme 2.2). At first, the substrates FO and NADP bind to the active site of both subunits of the homodimeric Fno. This causes a conformational change where the symmetric subunits yield an intermediate asymmetric dimer, such as described by Koshland as well as Miller. As a result of the conformational change, the second subunit becomes more difficult to reduce (negative cooperativity). Therefore, the hydride transfer occurs in the first subunit (half-site reactivity), followed by the second subunit hydride transfer. Given that the pre steady-state kinetic results reveal burst kinetics, it is plausible that the slow step could be product release, protonation of the nitrogen at position 1, or conformational changes

within Fno. To get an in depth understanding of the slow step, additional experiments need to be conducted to rule out some possibilities.

To understand the mechanism behind negative cooperativity and half site reactivity of *wt*Fno, we observed the Fno crystal structure very closely that showed the active site connectivity (Figure 2.9). Two amino acid residue His133 and Thr192 located adjacent to the C5 atom of F_{420} cofactor which would be the possible location of hydride transfer, but there is no evidence of forming H-bonds with any oxygen or ring nitrogen is seen. The nitrogen of thr192 residue forms a H-bond with the oxygen of main chain Ser190, which is at the interface of subunits. The ser190 side chain oxygen, forms a H-bond with another interface residue, arg186. The arg186 side chains amino group for both subunits could form H-bond with the ser190 side chain oxygen on both subunits. We propose the subunit-subunit interaction at the interface gives the molecular basis for inter-subunit communication during catalysis. It also plays an important regulatory role in the negative cooperativity kinetic studies in *wt*Fno.

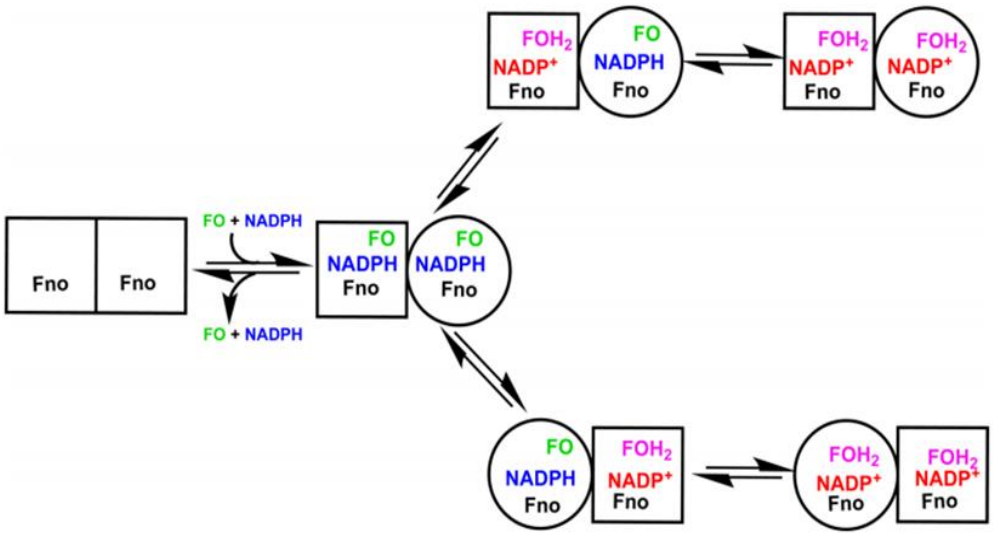

Scheme 2.2: Proposed scheme of *wt*Fno mechanism. According to this model, the hydride transfer reaction from NADPH to FO occurs at the first subunit. When the product is released from the first subunit, the hydride transfer will occur to the second subunit. Upon release of product, the first subunit will again re-engaged for the reaction

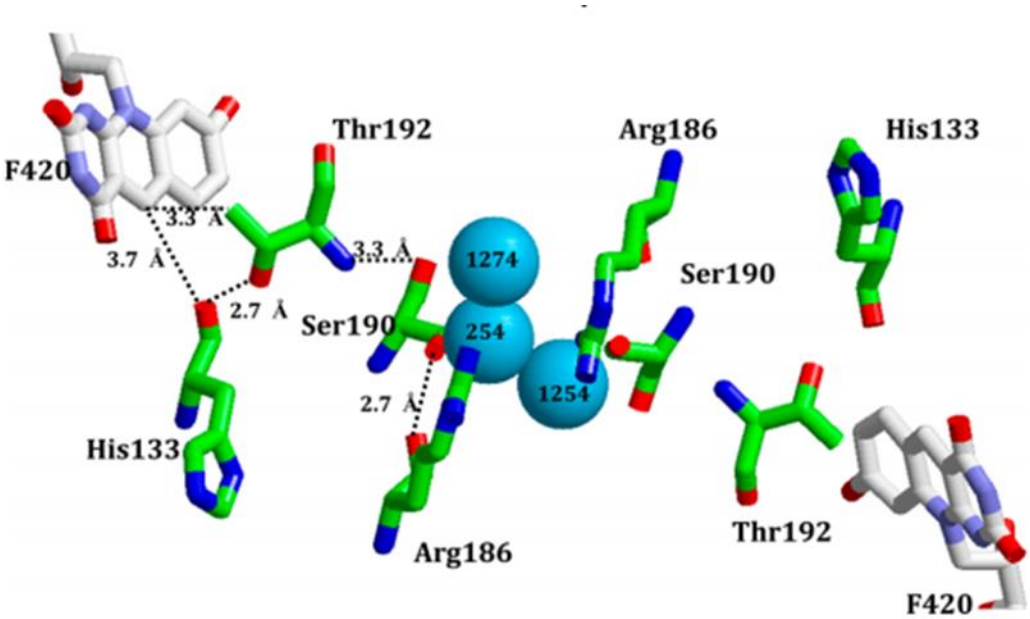

Figure 2.9: Crystal structure of Fno active site with mentioning the hydrogen bonding interactions involved with the active sites (53). Serine 190, Arginine 186 and 3 water molecules are at the interface of active sites. Serine 190 is connected with Threonine 192 through a hydrogen bonding at the subunit interface. Serine 190 has also hydrogen bonding interactions with Arginine 186.

Chapter 3

Increased hydride transfer rates within T09A Fno

3.1 Introduction

The crystal structure of F_{420}:H_2 $NADP^+$ oxidoreductase (Fno) published by Warkentin *et al*. (46) showed a conserved amino acid residue, Threonine 09 (T09) located at the vicinity of the coenzyme $NADP^+$. The distance between the hydroxyl group of T09 and the phosphate group of $NADP^+$ is 2.6 Å and ribose 2.9 Å. According to Jeffry *et al*. the mean donor acceptor distance for hydrogen bonding in proteins is 3.0 Å (54). They classified hydrogen bonding into 3 different types based on the donor acceptor distance, (i) 2.2 Å – 2.5 Å strong and mostly covalent (ii) 2.6 Å -3.2 Å moderate, mostly electrostatic and (iii) 3.2 Å – 4.0 Å weak electrostatic. So, based on this classification, the hydrogen bonding between hydroxyl group of T09 and phosphate group and also ribose of $NADP^+$ should be moderately strong and mostly electrostatic (54).

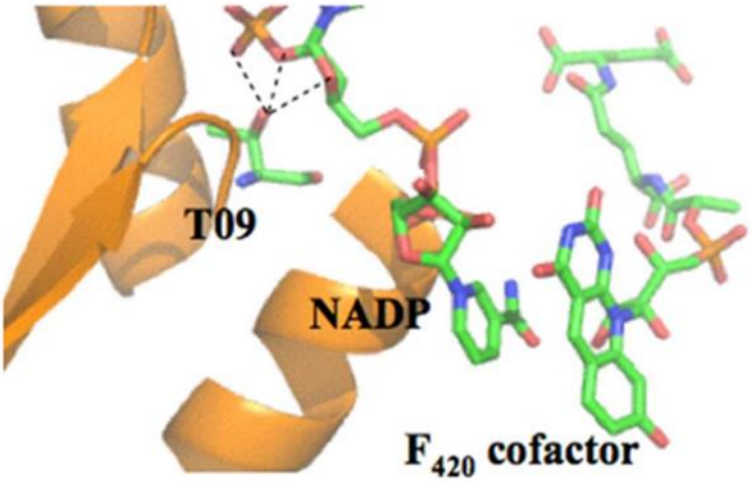

Figure 3.1: Position of Threonine 09 and $NADP^+$ within the active site of Fno (pdb 1jax). Threonine 09 has hydrogen bonding interactions with the phosphate group as well as ribose sugar of $NADP^+$.

The close proximity of the hydroxyl group of T09 and phosphate and ribose group of $NADP^+$ lead us to think about the presence of the hydrogen bonding and other ionic interactions. Considering those facts, we selected to study the role of this specific amino acid.

We created the T09A Fno variant, which doesn't contain the hydroxyl group. Binding, steady-state and pre steady-state kinetic experiments were conducted to study the functionality of T09 within Fno enzyme.

3.2 Materials and methods.

3.2.1 Reagents

FO was synthesized using a newly developed convenient synthesis method (45). The pET24b plasmid was purchased from Novagen. Isopropyl β-D-1-thiogalactopyranoside (IPTG) and E. coli C41DE3 cells were purchased from Gold Biotechnology and Lucigen respectively. Sodium chloride was purchased from Technova. NADPH, Sodium dodecyl sulfate, MES buffer and Ezrun protein marker were purchased from Akron Biotech, MP Biologics, Acros-Organics and Fisher Bioreagents respectively. Yeast extract, Tryptone, Kanamycin, Tris buffer, Ammonium sulfate and Potassium phosphate monobasic and dibasic buffer were purchased from Fisher Scientific. Bradford assay was purchased from Sigma-Aldrich.

3.2.2 Mutagenesis.

The cloning of the Fno gene (Figure 3.2) into pET24b plasmid was performed by Genescript. Site directed mutagenesis was conducted according to the Stratagene Agilent Quikchange manufacturer's protocol. The mutated gene sequence was verified by Sequetech (Mountain View, CA). The designed primer sequence is shown below (Table 3.1).

Table 3.1: Primer designed for T09A Fno.

Enzyme	**Sequence (5'-3')**
*wt*Fno	5' CTG CTG GGC GGT **ACG** GGC AAC CTG 3'
T09A Fno	5' CTG CTG GGC GGT **GCG** GGC AAC CTG 3'

DNA/Protein Sequence
CATATG (NdeI)

```
CGT GTG GCT CTG CTG GGC GGT ACG GGC AAC CTG GGC AAA GGT CTG GCA CTG CGT CTG
 R   V   A   L   L   G   G   T   G   N   L   G   K   G   L   A   L   R   L

GCA ACC CTG GGT CAT GAA ATC GTG GTC GGC TCA CGT CGC GAA GAA AAA GCG GAA GCC
 A   T   L   G   H   E   I   V   V   G   S   R   R   E   E   K   A   E   A

AAA GCG GCC GAA TAT CGT CGC ATT GCA GGC GAT GCT TCG ATC ACC GGT ATG AAA AAC
 K   A   A   E   Y   R   R   I   A   G   D   A   S   I   T   G   M   K   N

GAA GAC GCA GCT GAA GCG TGC GAT ATT GCC GTG CTG ACC ATC CCG TGG GAA CAT GCA
 E   D   A   A   E   A   C   D   I   A   V   L   T   I   P   W   E   H   A

ATT GAC ACG GCT CGT GAT CTG AAA AAT ATT CTG CGC GAA AAA ATC GTT GTT AGT CCG
 I   D   T   A   R   D   L   K   N   I   L   R   E   K   I   V   V   S   P

CTG GTG CCG GTT TCC CGT GGT GCC AAA GGT TTT ACC TAC AGC TCT GAA CGC TCA GCG
 L   V   P   V   S   R   G   A   K   G   F   T   Y   S   S   E   R   S   A

GCC GAA ATT GTT GCC GAA GTC CTG GAA AGC GAA AAA GTC GTG TCT GCC CTG CAC ACG
 A   E   I   V   A   E   V   L   E   S   E   K   V   V   S   A   L   H   T

ATC CCG GCA GCT CGT TTT GCA AAC CTG GAT GAA AAA TTC GAC TGG GAT GTC CCG GTG
 I   P   A   A   R   F   A   N   L   D   E   K   F   D   W   D   V   P   V

TGT GGC GAT GAC GAT GAA AGC AAA AAA GTT GTC ATG TCA CTG ATT TCG GAA ATT GAT
 C   G   D   D   D   E   S   K   K   V   V   M   S   L   I   S   E   I   D

GGT CTG CGT CCG CTG GAT GCC GGT CCG CTG AGT AAT TCC CGC CTG GTT GAA TCT CTG
 G   L   R   P   L   D   A   G   P   L   S   N   S   R   L   V   E   S   L

ACG CCG CTG ATT CTG AAC ATT ATG CGT TTT AAC GGT ATG GGC GAA CTG GGT ATC AAA
 T   P   L   I   L   N   I   M   R   F   N   G   M   G   E   L   G   I   K

TTT CTG TGA      GGATCC
 F   L   (stop)  (BamHI)
```

Figure 3.2: Complete *wt*Fno sequence.

3.2.3 Expression and purification.

The T09A Fno was expressed and purified according to the previously published optimized purification protocol of *wt*Fno with slight modification (52). The dialysis buffer used for *wt*Fno purification was 20 mM Tris-HCl at pH 7.5 in presence of 50 mM NaCl. Here we used 20 mM Tris-HCl, pH 6.5 and changed the NaCl concentration into 100 mM. Purified enzyme concentration was measured according to the Bradford assay (55).

3.2.4 Binding of FO and NADPH to T09A Fno

The binding studies of FO and NADPH to T09A Fno were performed using fluorescence spectroscopy (Horiba Fluoromax spectrophotometer) at room temperature (22 ° C). To determine the dissociation constant of FO, 0.2 µM T09A Fno was titrated with varying concentrations of FO in 50 mM MES/NaOH buffer, pH 6.5. The sample was excited at 290 nm and the emission scans were done at 320 nm to 800 nm. The binding assays were monitored using a spectrosil quarts submicro cell (purchased from Sterna). NADPH binding was performed in a similar fashion using 0.2 µM T09A Fno, titrated with varying concentration of NADPH in 50 mMMES/NaOH buffer at pH 6.5.

The slit width of excitation and emission were 4 and 8 nm respectively. After exciting the sample at 290 nm, a decrease in tryptophan emission was observed both for NADPH and FO, which was used to determine the K_d of FO and NADPH (Muller and Denicola 2002) . A concentration versus the normalized fluorescence plot was drawn to measure the K_d. The plot was fitted into Adair equation (57) (equation 1).

$$\Delta F = [F_{max} [L]/(K_d + [L])] \quad (1)$$

Here, ΔF is the change of fluorescence at 340 nm caused by FO or NADPH ligands [L], F_{max} is the normalized maximum fluorescence and K_d is the dissociation constant.

3.2.5 Steady-state kinetics.

Steady-state kinetic studies of T09A were conducted using Varian Cary 100 Bio UV-Vis spectrophotometer. All the studies were performed at room temperature (22° C). 50 mM MES/NaOH buffer, pH 6.5 was used as reaction buffer. To measure the kinetic parameters of FO, the concentration of FO was varied and NADPH concentration was fixed at 600 µM in presence of 10 nM T09A Fno (final concentration). To determine kinetic parameters of NADPH, the NADPH concentration was varied and FO concentration was fixed (25 µM) in presence of 10 nM T09A Fno (final concentration). The concentration of FO was measured using the extinction coefficient of 41.4 $mM^{-1}cm^{-1}$ at 420 nm in phosphate buffer pH 7.0. On the other hand NADPH concentration was measured with the extinction coefficient 6.22 mM-1cm-1 at 340 nm in Tris-HCl buffer, pH 7.4. The rate was converted from µM s^{-1} to s^{-1} by dividing the enzyme concentration.

A concentration versus rate curve was drawn to find the kinetic parameters. To find the parameters for FO, the curve was fitted into classical Michaelis-Menten equation (hyperbola) using Sigmaplot 13.0 (equation 2).

$$k = k_{cat}\,[S]/(K_m+[S]) \qquad (2)$$

However, the data varying NADPH concentration does not fit into the same equation. We had to fit it into bi-phasic Michaelis-Menten equation (equation 3).

$$k = k_{cat}1[S]/(K_m1+[S]) + k_{cat}2[S]/(K_m2 + [S]) \qquad (3)$$

Here, k is the first-order macroscopic rate constant, K_m is the Michaelis-Menten constant, [S] is the substrate concentration and k_{cat} is the turnover number.

3.2.6 Pre steady-state kinetics.

The pre steady-state kinetic studies were performed using a Hitech Scientific DX2 stopped-flow spectrophotometer at 22 °C. T09A Fno (1.0, and 2.0 µM of T09A Fno

with 50 mM MES/NaOH buffer, pH 6.5) was mixed with 25 μM FO, which forms the T09A Fno-FO complex. 10 μM NADPH was then mixed with T09A Fno-FO complex to form T09A Fno-NADPH complex. The reduction of FO was monitored by analyzing the change of absorbance at 420 nm.

The data were then fitted to a single exponential decay equation (equation 4), using Sigmaplot 13.0

$$\text{Absorbance} = A_0\, e^{(k_{obs}\, t)} + c \qquad (4)$$

Here, A_0 is the amplitude of the burst, k_{obs} is the observed rate constant and c is the non-zero baseline.

3.2.7 Circular dichroism (CD)

Circular dichroism (CD) was used to compare the secondary structure of *wt*Fno and T09A Fno. 5 μM *wt*Fno with10 nM phoshphate buffer pH 7.0 was used conduct this study. In the same way 5 μM T09A Fno with 10 nM phosphate buffer was used to perform the study. The obtained data were analyzed by Capito, a web server based CD data analysis tool (58) at http://capito.nmr.leibniz-fli.de/ .

3.3 Results and discussion

Based upon our collected data, the T09A K_d for FO is similar to *wt*Fno (Table 3.2, Figures 3.3 & 3.4). However, the T09A K_d for NADPH displayed a 5-fold increase in comparison to *wt*Fno . The steady-state kinetic data of T09A varying FO concentration displayed the classical Michaelis-Menten characteristics, as what was observed with *wt*Fno . While the k_{cat} value is similar to *wt*Fno , the K_m for FO is double that of *wt*Fno (Table 3.2).

Table 3.2: Comparison of the dissociation constants (K_d) of T09A Fno with *wt*Fno . The *wt*Fno data used from previously published article (53).

	K_d (T09A Fno)	**K_d (*wt*Fno)**
FO	4.9 ± 0.6 nM	3.6 ± 0.7 nM
NADPH	10.9 ± 1.3 nM	2.0 ± 0.3 nM

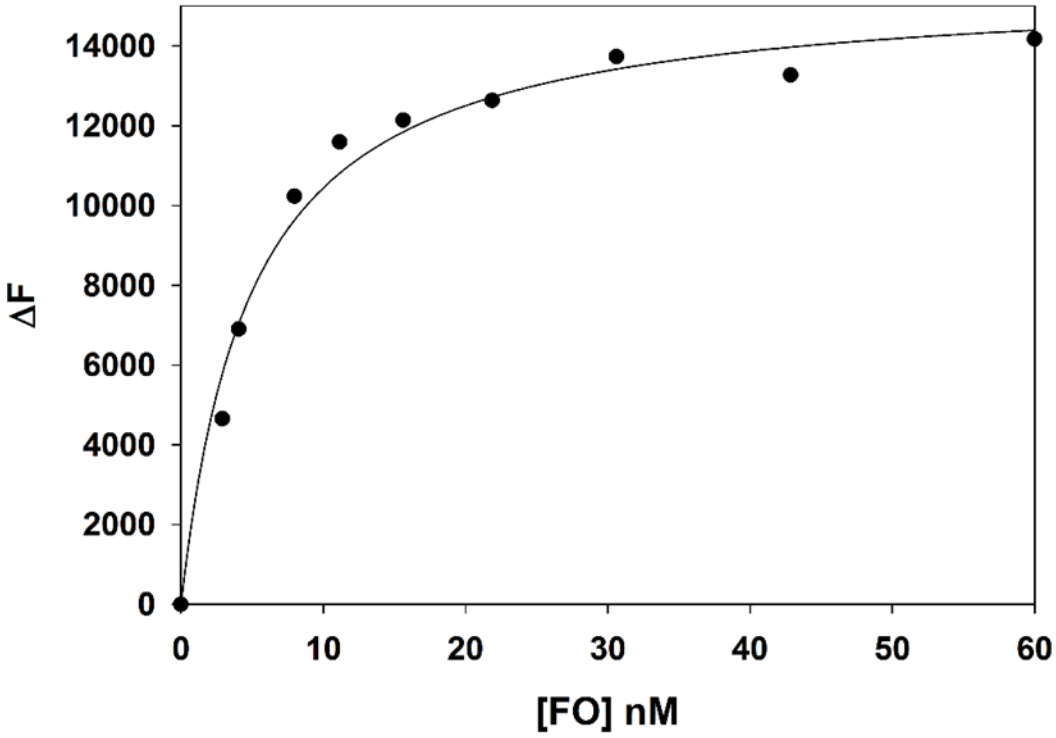

Figure 3.3: Binding of FO to the T09A Fno mutant enzyme. Here, ΔF denotes the change of fluorescence at 340 nm. The actual fluorescence values were inverted and normalized before plotting into Adair equation. The experiment was done at 50 mM MES/NaOH buffer pH 6.5. T09A Fno concentration was 0.2 µM and the study was done at room temperature. The plot was fitted into Adair equation (equation 1).

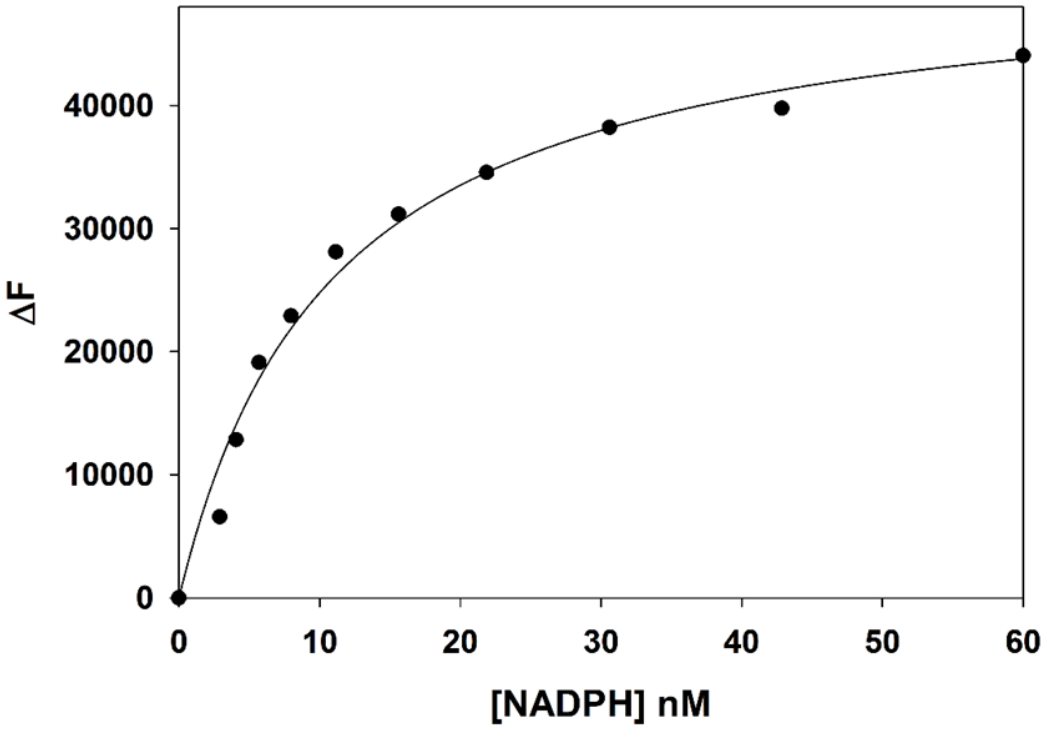

Figure 3.4: Binding studies of T09A Fno by varying NADPH concentration. Here, ΔF denotes the change of fluorescence at 340 nm. The actual fluorescence values were inverted and normalized before fitting into Adair equation. Reaction buffer was 50 mM MES/NaOH, pH 6.5 and 0.2 μM T09A Fno were used for it. The study was conducted at room temperature. The plot was fitted into Adair equation (equation 1).

Here, the K_m for FO is significantly higher than its K_d. The binding studies were conducted with either FO and T09A Fno or NADPH and T09A Fno, only one substrate present for each study. However, the steady-state kinetic studies were conducted in presence of both FO and NADPH with the T09A Fno variant. K_d value only depends on

the kinetic parameters k_{on} and k_{off}, however K_m is dependent upon k_{on}, k_{off} as well as k_{cat} parameters, which causes the difference between K_d and K_m.

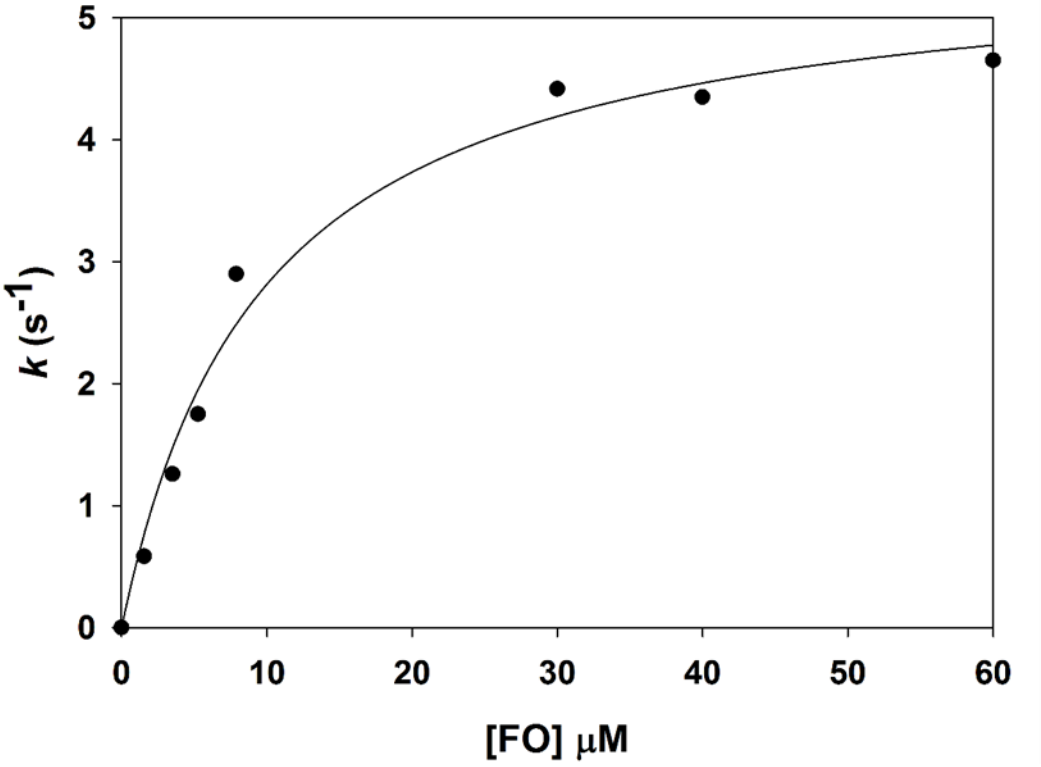

Figure 3.5: Steady-state kinetics of T09A Fno, varying FO. The reaction was carried out at 50 mM MES/NaOH buffer, pH 6.5. NADPH and T09A concentration were constant, 600 μM and 10 nM respectively. FO concentration was varied from 0-60 μM. The study was conducted at room temperature (22 °C). Data were fitted into Michaelis-Menten equation (equation 2).

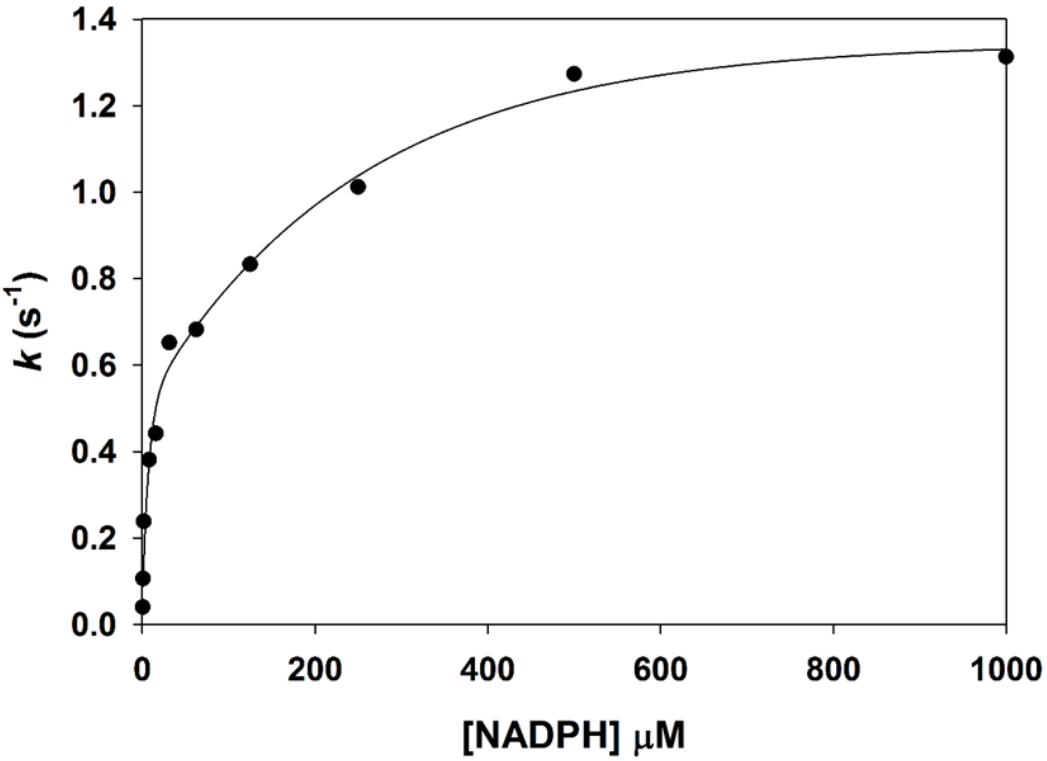

Figure 3.6: Steady-state kinetic studies of T09A Fno varying NADPH concentration from 0-1000 µM. FO concentration was constant at 25 µM. T09A Fno concentration was 10 nM, reaction buffer was 50 mM MES/NaOH, pH 6.5 and the reaction temperature was 22 °C. Data were fitted into bi-phasic hyperbola equation (equation 3).

The steady-state kinetics of varying NADPH concentrations displayed similar biphasic characteristics as *wt*Fno , with a K_m comparable to *wt*Fno for the first phase (Table 3.3). However, the second phase K_m increased significantly. The T09A k_{cat} value for varying NADPH is significantly lower than the k_{cat} parameter varying FO concentrations for this mutant.

Table 3.3: K_m and k_{cat} values for FO and NADPH of T09A Fno compared to *wt*Fno . The data for *wt*Fno is from our recently published article (53).

	k_{cat} (s^{-1})		K_m (µM)	
	T09A Fno	***wt*Fno**	**T09A Fno**	***wt*Fno**
FO	5.54 ± 0.29	5.27 ± 0.14	9.70 ± 1.6	4.00± 0.39
NADPH Phase 1	N/A	N/A	2.20 ± 0.82	2.33 ± 0.19
NADPH Phase 2	1.10 ± 0.06	5.41 ± 0.04	197 ± 48	61.6 ± 5.9

This was not seen with *wt*Fno . For example, the k_{cat} values for *wt*Fno with varying FO and NADPH concentrations are similar, with no preference for which cofactor is added first. However, the T09A Fno variant requires the presence of NADPH prior to the introduction of FO for optimal catalytic activity. Based upon our *wt*Fno FO binding studies, which was performed in the presence of $NADP^+$, as well as without $NADP^+$, there was no change in the affinity of the enzyme for FO in either case . This suggests that *wt*Fno does not require the presence of NADPH first. Additionally, the pre steady-state data suggests that the hydride transfer rate is not affected by which cofactor is present first for the variant. It appears that the slow phase is affected, based upon the differences in k_{cat}.

Unlike *wt*Fno , which displayed an initial burst and then a slow phase, the T09A variant pre steady-state data showed a single phase exponential decay (Figure 3.7). The slow phase cannot be observed within this variant on the stopped flow. The rate of hydride transfer (burst phase) was 36 times faster than *wt*Fno (Table 3.4). Additionally, the amplitude of the burst phase corresponds to ~100% of FO reduction, rather than 50% as observed with *wt*Fno and I135 variants (data not shown).

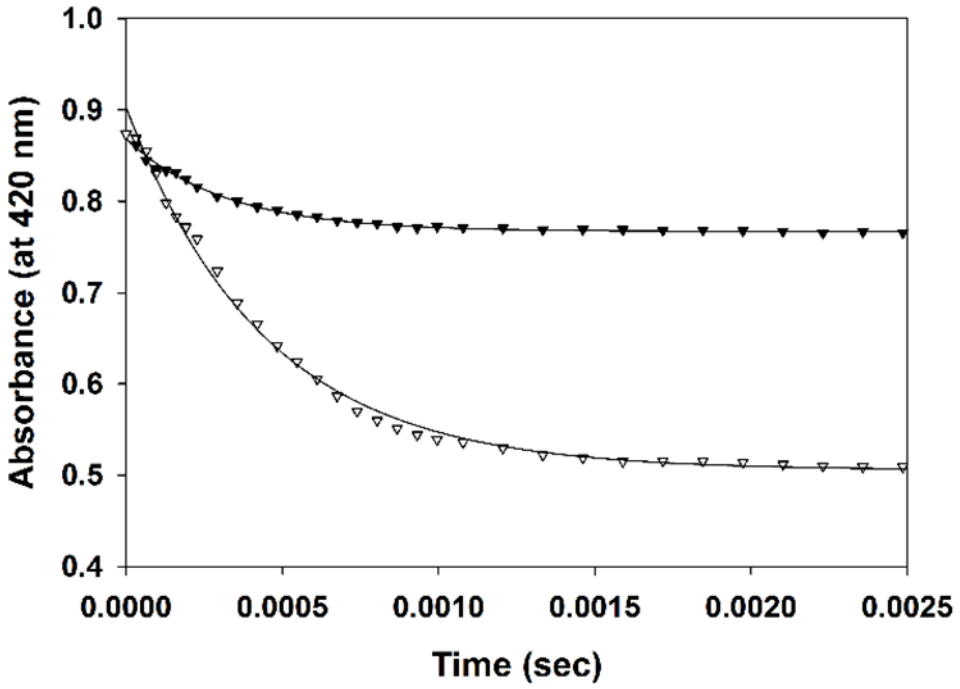

Figure 3.7: Pre steady-state kinetic studies on different concentrations of T09A Fno. The solid triangles and opened triangles represent for reaction with 1 µM and 2 µM T09A respectively. The reactions were conducted in 50 mM MES/NaOH buffer, pH 6.5 with 25 µM FO and 10 µM NADPH. Reactions were conducted at 22° C. Data were fitted into single exponential decay equation (equation 4).

Table 3.4: Comparison of the rate constants (k_{obs}) of T09A Fno with *wt*Fno . *wt*Fno data from our previously published article (53).

	Rate constant (k_{obs})
T09A Fno	3140 ± 34 s^{-1}
*wt*Fno	87 ± 2 s^{-1}

Circular dichroism (CD) was conducted to check the secondary structure of the mutant. The data were compared with the *wt*Fno to see any possible changes in secondary structure due to the mutation. CD was performed with 5 µM T09A Fno and 5 µM *wt*Fno separately and the obtained data were analyzed using CAPITO, a web server based CD data analysis software (figure 3.9).

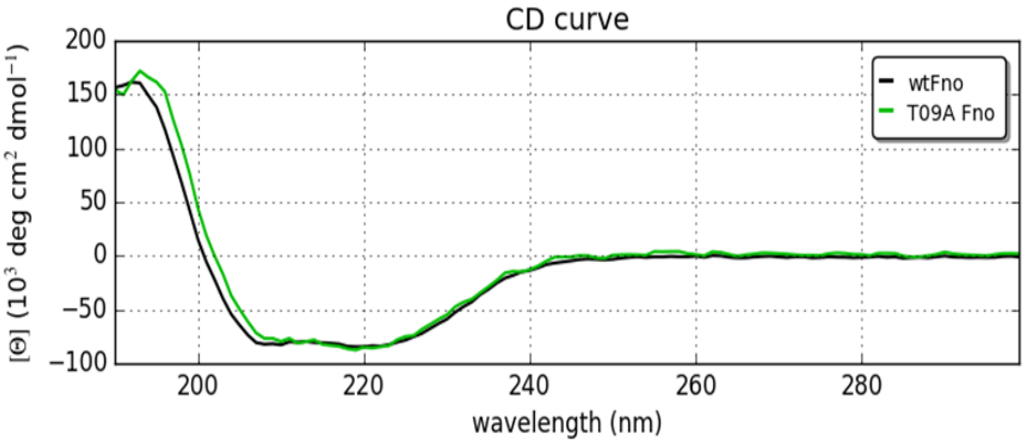

Figure 3.9: Circular dichroism spectra of *wt*Fno vs T09A Fno. The concentrations used were 5 µM for both *wt*Fno and T09A Fno in 10 mM Phosphate buffer, pH 7.0. The study was conducted at room temperature (22 °C). Here, the green line represents the spectra of T09A Fno and black line represents for *wt*Fno, Θ represents the molar ellipticity, which

is a function of wavelength λ. The plot was made with the web server based CD spectra analysis software CAPITO (58).

There was no significant difference observed between the CD spectra of *wt*Fno and T09A Fno. This data refers to that, there is no significant change occurred on the secondary structure due to the mutation of T09 position. However, these spectra were found in resting state of the wild type enzyme and the mutant, so the possibility of conformational change still remains in presence of substrates.

3.4 Conclusion

The binding experiments revealed that T09A Fno does not affect FO binding, but plays a major role in NADPH binding. This is consistent with what is seen within the Fno crystal structure, given the 2.6 Å distances between the hydroxyl group of T09 and the phosphate of NADPH. The interaction of T09 with the ribose oxygen is 2.9 Å. T09 also helps to position NADP appropriately

within the active site. The increased rate of hydride transfer with T09A Fno variant suggests that the T09 residue plays a role in the rate at which the hydride is transferred, therefore aiding in the regulation of NADPH within Fno. In our previous studies with *wt*Fno , we suggested that Fno is a regulatory enzyme that undergoes ligand-induced conformational changes that affect subunit interactions. Should NADPH change positions within the active site of Fno, due to the loss of the T09 hydrogen bonding with the phosphate group of NADPH and the ribose, this could affect the subunit interactions as well as the cooperativity kinetics. Converting the threonine into an alanine, creates additional space within the active site. This could trigger Fno to undergo a large scale conformational change to bring the two cofactors closer together, thereby

speeding up the rate of the hydride transfer. Given the loss of cooperativity, T09 may be a residue that is involved with subunit communication.

References

1. Taylor, M., Scott, C., and Grogan, G. (2013) F_{420}-dependent enzymes - potential for applications in biotechnology. *Trends Biotechnol.* **31**, 63–64
2. Kern, R., Keller, P. J., Schmidt, G., and Bacher, A. (1983) Isolation and structural identification of a chromophoric coenzyme F_{420} fragment from culture fluid of *Methanobacterium thermoautotrophicum*. *Arch. Microbiol.* **136**, 191–193
3. Yamazaki, S., and Tsai, L. (1980) Purification and properties of 8-hydroxy-5-deazaflavin-dependent $NADP^+$ reductase from *Methanococcus vannielii*. *J. Biol. Chem.* **255**, 6462–6465
4. Jones, J. B., and Stadtman, T. C. (1980) Reconstitution of a formate- $NADP^+$ oxidoreductase from formate dehydrogenase and a 5-deazaflavin-linked $NADP^+$ reductase isolated from *Methanococcus vannielii. J. Biol. Chem.* **255**, 1049–1053
5. Jacobson, F. S., Daniels, L., Fox, J. A., Walsh, C. T., and Orme-Johnson, W. H. (1982) Purification and properties of an 8-hydroxy-5-deazaflavin-reducing hydrogenase from *Methanobacterium thermoautotrophicum*. *J. Biol. Chem.* **257**, 3385–3388
6. Hartzell, P. L., Zvilius, G., Escalante-Semerena, J. C., and Donnelly, M. I. (1985) Coenzyme F_{420} dependence of the methylenetetrahydromethanopterin dehydrogenase of *Methanobacterium thermoautotrophicum*. *Biochem. Biophys. Res. Commun.* **133**, 884–890
7. Widdel, F., and Wolfe, R. S. (1989) Expression of secondary alcohol dehydrogenase in methanogenic bacteria and purification of the F_{420}-specific enzyme from *Methanogenium thermophilum* strain TCI. *Arch. Microbiol.* **152**, 322–328

8. DiMarco, A. A., Bobik, T. A., and Wolfe, R. S. (1990) Unusual coenzymes of methanogenesis. *Annu. Rev. Biochem.* **59**, 355–394

9. Kunow, J., Schwörer, B., Stetter, K. O., and Thauer, R. K. (1993) A F_{420}-dependent NADP reductase in the extremely thermophilic sulfate-reducing *Archaeoglobus fulgidus*. *Arch. Microbiol.* **160**, 199–205

10. Eker, A. P. M., Hessels, J. K. C., and Van de Velde, J. (1988) Photoreactivating enzyme from the green alga *Scenedesmus acutus*. Evidence for the presence of two different flavin chromophores. *Biochemistry*. **27**, 1758–1765

11. Eker, A. P., Kooiman, P., Hessels, J. K., and Yasui, A. (1990) DNA photoreactivating enzyme from the cyanobacterium *Anacystis nidulans*. *J. Biol. Chem.* **265**, 8009–8015

12. Rhodes, P. M., Winskill, N., Friend, E. J., and Warren, M. (1981) Biochemical and genetic characterization of *Streptomyces rimosus* mutants impaired in oxytetracycline biosynthesis. *Microbiology*. **124**, 329–338

13. McCormick, J. R. D., and Morton, G. O. (1982) Identity of cosynthetic factor I of Streptomyces aureofaciens and fragment FO from coenzyme F_{420} of *Methanobacterium* species. *J. Am. Chem. Soc.* **104**, 4014–4015

14. Cheeseman, P., Toms-Wood, A., and Wolfe, R. S. (1972) Isolation and properties of a fluorescent compound, Factor420, from *Methanobacterium* strain MoH. *J. Bacteriol.* **112**, 527–531

15. Eirich, L. D., Vogels, G. D., and Wolfe, R. S. (1978) Proposed structure for coenzyme F_{420} from *Methanobacterium*. *Biochemistry*. **17**, 4583–4593

16. Bair, T. B., Isabelle, D. W., and Daniels, L. (2001) Structures of coenzyme F_{420} in *Mycobacterium* species. *Arch. Microbiol.* **176**, 37–43

17. Tzeng, S. F., Bryant, M. P., and Wolfe, R. S. (1975) Factor 420-Dependent Pyridine Nucleotide-Linked Formate Metabolism of *Methanobacterium rum inantium*. *J. Bacteriol.* **121**, 192–196

18. Teshima, T., Nakaji, A., Shiba, T., Tsai, L., and Yamazaki, S. (1985) Elucidation of stereospecificity of a selenium-containing hydrogenase from *Methanococcus vannielii*—syntheses of (R)-and (S)-[4-2 H 1] 3, 4-dihydro-7-hydroxy-1-hydroxyethylquinolinone. *Tetrahedron Lett.* **26**, 351–354

19. Fox, J. A., Livingston, D. J., Orme-Johnson, W. H., and Walsh, C. T. (1987) 8-Hydroxy-5-deazaflavin-reducing hydrogenase from *Methanobacterium thermoautotrophicum*: 1. Purification and characterization. *Biochemistry*. **26**, 4219–4227

20. Michel, R., Massanz, C., Kostka, S., Richter, M., and Fiebig, K. (1995) Biochemical Characterization of the 8-hydroxy-5-deazaflavin-reactive Hydrogenase from *Methanosarcina barkeri* Fusaro. *Eur. J. Biochem.* **233**, 727–735

21. Schauer, N. L., and Ferry, J. G. (1986) Composition of the coenzyme F_{420}-dependent formate dehydrogenase from *Methanobacterium formicicum*. *J. Bacteriol.* **165**, 405–411

22. Klein, A. R., Berk, H., Purwantini, E., Daniels, L., and Thauer, R. K. (1996) Si-Face Stereospecificity at C5 of Coenzyme F_{420} for F_{420}-Dependent Glucose-6-Phosphate Dehydrogenase from *Mycobacterium smegmatis* and F_{420}-Dependent Alcohol Dehydrogenase from *Methanoculleus thermophilicus*. *Eur. J. Biochem.* **239**, 93–97

23. Hagemeier, C. H., Shima, S., Warkentin, E., Thauer, R. K., and Ermler, U. (2003) Coenzyme F_{420}-dependent methylenetetrahydromethanopterin dehydrogenase

from *Methanopyrus kandleri*: the selenomethionine-labelled and non-labelled enzyme crystallized in two different forms. *Acta Crystallogr. Sect. D Biol. Crystallogr.* **59**, 1653–1655

24. Shima, S., Warkentin, E., Grabarse, W., Sordel, M., Wicke, M., Thauer, R. K., and Ermler, U. (2000) Structure of coenzyme F 420 dependent methylenetetrahydromethanopterin reductase from two methanogenic archaea. *J. Mol. Biol.* **300**, 935–950

25. Beifuss, U., Tietze, M., Bäumer, S., and Deppenmeier, U. (2000) Methanophenazine: structure, total synthesis, and function of a new cofactor from methanogenic archaea. *Angew. Chemie Int. Ed.* **39**, 2470–2472

26. Berk, H., and Thauer, R. K. (1998) F RPH H P : NADP oxidoreductase from *Methanobacterium thermoautotrophicum* : identification of the encoding gene via functional overexpression in Escherichia coli. **438**, 124–126

27. Aufhammer, S. W., Warkentin, E., Berk, H., Shima, S., Thauer, R. K., and Ermler, U. (2004) Coenzyme binding in F 420-dependent secondary alcohol dehydrogenase, a member of the bacterial luciferase family. *Structure*. **12**, 361–370

28. Purwantini, E., and Daniels, L. (1996) Purification of a novel coenzyme F_{420}-dependent glucose-6-phosphate dehydrogenase from *Mycobacterium smegmatis*. *J. Bacteriol.* **178**, 2861–2866

29. Kiener, A., Husain, I., Sancar, A., and Walsh, C. (1989) Purification and properties of *Methanobacterium thermoautotrophicum* DNA photolyase. *J. Biol. Chem.* **264**, 13880–13887

30. O'Connor, K. A., McBride, M. J., West, M., Yu, H., Trinh, L., Yuan, K., Lee, T., and Zusman, D. R. (1996) Photolyase of *Myxococcus xanthus*, a Gram-negative

eubacterium, is more similar to photolyases found in Archaea and higher eukaryotes than to photolyases of other eubacteria. *J. Biol. Chem.* **271**, 6252–6259

31. Komori, H., Masui, R., Kuramitsu, S., Yokoyama, S., Shibata, T., Inoue, Y., and Miki, K. (2001) Crystal structure of thermostable DNA photolyase: pyrimidine-dimer recognition mechanism. *Proc. Natl. Acad. Sci.* **98**, 13560–13565
32. Eker, A. P. M., Yajima, H., and Yasui, A. (1994) DNA photolyase from the fungus *Neurospora crassa*. Purification, characterization and comparison with other photolyases. *Photochem. Photobiol.* **60**, 125–133
33. McCready, S., and Marcello, L. (2003) Repair of UV damage in Halobacterium salinarum. *Biochem. Soc. Trans.* **31**, 694–698
34. Vermeij, P., Detmers, F. J. M., Broers, F. J. M., Keltjens, J. T., and Drift, C. (1994) Purification and Characterization of Coenzyme F390 Synthetase from *Methanobacterium thermoautotrophicum* (strain□ H). *Eur. J. Biochem.* **226**, 185–191
35. Vermeij, P., van der Steen, R. J., Keltjens, J. T., Vogels, G. D., and Leisinger, T. (1996) Coenzyme F390 synthetase from *Methanobacterium thermoautotrophicum* Marburg belongs to the superfamily of adenylate-forming enzymes. *J. Bacteriol.* **178**, 505–510
36. Kengen, S. W., Von den Hoff, H. W., Keltjens, J. T., Van der Drift, C., and Vogels, G. D. (1991) F390 synthetase and F390 hydrolase from *Methanobacterium thermoautotrophicum* (strain delta H). *Biofactors*. **3**, 61–65
37. Vermeij, P., Vinke, E., Keltjens, J. T., and Drift, C. (1995) Purification and properties of coenzyme F390 hydrolase from *Methanobacterium thermoautotrophicum* (strain Marburg). *Eur. J. Biochem.* **234**, 592–597

38. Seedorf, H., Dreisbach, A., Hedderich, R., Shima, S., and Thauer, R. K. (2004) $F_{420}H_2$ oxidase (FprA) from Methanobrevibacter arboriphilus, a coenzyme F_{420}-dependent enzyme involved in O_2 detoxification. *Arch. Microbiol.* **182**, 126–137

39. Walsh, C. (1986) Naturally occurring 5-deazaflavin coenzymes: biological redox roles. *Acc. Chem. Res.* **19**, 216–221

40. White, R. H. (2001) Biosynthesis of the methanogenic cofactors. *Vitam. Horm.* **61**, 299–337

41. Decamps, L., Philmus, B., Benjdia, A., White, R., Begley, T. P., and Berteau, O. (2012) Biosynthesis of F 0, precursor of the F 420 cofactor, requires a unique two radical-SAM domain enzyme and tyrosine as substrate. *J. Am. Chem. Soc.* **134**, 18173–18176

42. Philmus, B., Decamps, L., Berteau, O., and Begley, T. P. (2015) Biosynthetic versatility and coordinated action of 5′-deoxyadenosyl radicals in deazaflavin biosynthesis. *J. Am. Chem. Soc.* **137**, 5406–5413

43. Ashton, W. T., Brown, R. D., Jacobson, F., and Walsh, C. (1979) Synthesis of 7, 8-didemethyl-8-hydroxy-5-deazariboflavin and confirmation of its identity with the deazaisoalloxazine chromophore of *Methanobacterium* redox coenzyme F_{420}. *J. Am. Chem. Soc.* **101**, 4419–4420

44. Yoneda, F., Sakuma, Y., Ichiba, M., and Shinomura, K. (1976) Syntheses of isoalloxazines and isoalloxazine 5-oxides. A new synthesis of riboflavin. *J. Am. Chem. Soc.* **98**, 830–835

45. Hossain, M. S., Le, C. Q., Joseph, E., Nguyen, T. Q., Johnson-Winters, K., and Foss, F. W. (2015) Convenient synthesis of deazaflavin cofactor FO and its activity in F_{420} -dependent NADP reductase. *Org. Biomol. Chem.* **13**, 5082–5085

46. Warkentin, E., Mamat, B., Sordel-Klippert, M., Wicke, M., Thauer, R. K., Iwata, M., Iwata, S., Ermler, U., and Shima, S. (2001) Structures of $F_{420}H_2$: $NADP^+$ oxidoreductase with and without its substrates bound. *EMBO J.* **20**, 6561–6569

47. Koshland, D. E., Némethy, G., and Filmer, D. (1966) Comparison of experimental binding data and theoretical models in proteins containing subunits. *Biochemistry*. **5**, 365–385

48. De Wit, L. E. A., and Eker, A. P. M. (1987) 8-Hydroxy-5-deazaflavin-dependent electron transfer in the extreme halophile *Halobacterium cutirubrum*. *FEMS Microbiol. Lett.* **48**, 121–125

49. Elias, D. A., Juck, D. F., Berry, K. A., and Sparling, R. (2000) Purification of the NADP + : F 420 oxidoreductase of *Methanosphaera stadtmanae*. **420**, 998–1003

50. Eker, A. P. M. (1980) Photoreactivating enzyme from *Streptomyces griseus*—III. Evidence for the presence of an intrinsic chromophore. *Photochem. Photobiol.* **32**, 593–600

51. Almarsson, O., and Bruice, T. C. (1993) Evaluation of the factors influencing reactivity and stereospecificity in NAD (P) H dependent dehydrogenase enzymes. *J. Am. Chem. Soc.* **115**, 2125–2138

52. Le, C. Q., Joseph, E., Nguyen, T., and Johnson-Winters, K. (2015) Optimization of Expression and Purification of Recombinant Archeoglobus fulgidus $F_{420}H_2$:$NADP^+$ Oxidoreductase, an F_{420} Cofactor Dependent Enzyme. *Protein J.* **34**, 391–397

53. Joseph, E., Le, C. Q., Nguyen, T., Oyugi, M., Hossain, M. S., Foss, F. W., and Johnson-Winters, K. (2016) Evidence of Negative Cooperativity and Half-Site Reactivity within an F_{420} -Dependent Enzyme: Kinetic Analysis of $F_{420}H_2$:$NADP^+$ Oxidoreductase. *Biochemistry*. 10.1021/acs.biochem.5b00762

54. Jeffrey, G. A., and Jeffrey, G. A. (1997) *An introduction to hydrogen bonding*, Oxford university press New York

55. Bradford, M. M. (1976) A rapid and sensitive method for the quantitation of microgram quantities of protein utilizing the principle of protein-dye binding. *Anal. Biochem.* **72**, 248–254

56. Müller, M., and Denicola, A. (2002) Study of protein-ligand binding by fluorescence. *Biochem. Mol. Biol. Educ.* **30**, 309–312

57. Adair, G. S. (1925) The hemoglobin system VI. The oxygen dissociation curve of hemoglobin. *J. Biol. Chem.* **63**, 529–545

58. Wiedemann, C., Bellstedt, P., and Görlach, M. (2013) CAPITO-A web server based analysis and plotting tool for circular dichroism data. *Bioinformatics*

Biographical Information

Md Hasmat Ullah was born in October 01, 1986 in a village of Kapasia, Bangladesh. He earned his Bachelors and Masters in Biochemistry and Molecular Biology in 2010 and 2011 respectively, from Jahangirnagar University, Bangladesh. Then he came in USA and entered into the graduate program of Chemistry and Biochemistry department of the University of Texas at Arlington.

He worked in an enzyme kinetics research lab under the supervision of Dr. Kayunta Johnson-Winters. His research focus is on the hydride transfer mechanism of F_{420} dependent $NADP^+$ Oxidoreductase (Fno). His future plan is to be a recognized researcher in enzyme kinetics.